Monthly Notices
of the
ROYAL ASTRONOMICAL SOCIETY

Mon. Not. R. Astron. Soc. **426,** 1950–1958 (2012) doi:10.1111/j.1365-2966.2012.21773.x

An accurate mass and radius measurement for an ultracool white dwarf

S. G. Parsons,[1,2⋆] B. T. Gänsicke,[1] T. R. Marsh,[1] P. Bergeron,[3] C. M. Copperwheat,[1] V. S. Dhillon,[4] J. Bento,[1] S. P. Littlefair[4] and M. R. Schreiber[2]

[1]*Department of Physics, University of Warwick, Coventry CV4 7AL*
[2]*Departmento de Física y Astronomía, Universidad de Valparaíso, Avenida Gran Bretana 1111, Valparaíso, Chile*
[3]*Département de Physique, Université de Montréal, C.P. 6128, Succursale Centre-Ville, Montréal, QC H3C 3J7, Canada*
[4]*Department of Physics and Astronomy, University of Sheffield, Sheffield S3 7RH*

Accepted 2012 July 23. Received 2012 July 20; in original form 2012 June 15

ABSTRACT

Studies of cool white dwarfs in the solar neighbourhood have placed a limit on the age of the Galactic disc of 8–9 billion years. However, determining their cooling ages requires the knowledge of their effective temperatures, masses, radii and atmospheric composition. So far, these parameters could only be inferred for a small number of ultracool white dwarfs for which an accurate distance is known, by fitting their spectral energy distributions in conjunction with a theoretical mass–radius relation. However, the mass–radius relation remains largely untested, and the derived cooling ages are hence model dependent. Here we report direct measurements of the mass and radius of an ultracool white dwarf in the double-lined eclipsing binary SDSS J013851.54−001621.6. We find $M_{\rm WD} = 0.529 \pm 0.010\,{\rm M}_{\odot}$ and $R_{\rm WD} = 0.0131 \pm 0.0003\,{\rm R}_{\odot}$. Our measurements are consistent with the mass–radius relation and we determine a robust cooling age of 9.5 billion years for the 3570 K white dwarf. We find that the mass and radius of the low-mass companion star, $M_{\rm sec} = 0.132 \pm 0.003\,{\rm M}_{\odot}$ and $R_{\rm sec} = 0.165 \pm 0.001\,{\rm R}_{\odot}$, are in agreement with evolutionary models. We also find evidence that this >9.5 Gyr old M5 star is still active, far beyond the activity lifetime for a star of its spectral type. This is likely caused by the high tidally enforced rotation rate of the star. The companion star is close to filling its Roche lobe and the system will evolve into a cataclysmic variable in only 70 Myr. Our direct measurements demonstrate that this system can be used to calibrate ultracool white dwarf atmospheric models.

Key words: binaries: eclipsing – stars: fundamental parameters – stars: late-type – white dwarfs.

1 INTRODUCTION

White dwarfs are born hot and cool gradually over billions of years. Their cooling is understood well enough to make them useful in measuring the ages of stellar populations (Fontaine, Brassard & Bergeron 2001). White dwarfs with brown dwarf companions can be used to place constraints on the age of the brown dwarf (Pinfield et al. 2006; Day-Jones et al. 2008). The growing number of wide field surveys, such as the United Kingdom Infrared Telescope (UKIRT) Infrared Deep Sky Survey and the Sloan Digital Sky Survey (SDSS), have led to an increase in the number of these systems (Girven et al. 2011; Steele et al. 2011). A proper understanding of white dwarf cooling is essential for placing reliable limits on the ages of these systems.

White dwarf temperatures, and hence ages, are determined by fitting their spectral energy distributions (SEDs) using models of their atmospheres. At low temperatures ($T_{\rm eff} < 6000$ K) the atmospheric models need to include the effects of collisions between hydrogen molecules (Bergeron, Saumon & Wesemael 1995; Bergeron & Leggett 2002) (and with helium, if present). These effects dominate at near-infrared wavelengths in ultracool white dwarfs ($T_{\rm eff} < 4000$ K), suppressing the infrared flux and causing it to emerge at shorter wavelengths (Bergeron et al. 1994). In addition, the SEDs of ultracool white dwarfs depend on the white dwarf's surface gravity, and hence its mass and radius. Current white dwarf atmosphere models are not yet able to produce satisfying fits to the observed SEDs of ultracool white dwarfs (Giammichele, Bergeron & Dufour 2012).

If an accurate distance is known, the absolute magnitude and a mass–radius relation can be used in conjunction with the SED modelling to estimate the mass and the surface gravity of the star. However, parallaxes are available only for a small handful of ultracool white dwarfs. In one of the best-studied cases, LHS 3250, this method gives an unrealistically low surface gravity of $\log g = 7.27$, underlining the uncertainties in the SED models

⋆E-mail: steven.parsons@warwick.ac.uk

© 2012 The Authors
Monthly Notices of the Royal Astronomical Society © 2012 RAS

Table 1. Journal of photometric and spectroscopic observations. Exposure times for the X-shooter observations are for the UVB, VIS and NIR arms, respectively.

Date at start of run	Instrument	Filter(s)	Start (UT)	Orbital phase	Exposure time (s)	Conditions (transparency, seeing) (arcsec)
2011-11-01	ULTRACAM	*ugr*	23:51	0.90–2.25	4.0	Variable, ∼1
2011-11-30	RATCam	*r*	20:57	0.81–1.07	10.0	Good, ∼1.5
2011-11-30	RATCam	*i*	22:41	0.77–1.03	10.0	Good, ∼1.5
2011-12-01	RATCam	*r*	21:24	0.80–1.08	10.0	Good, ∼2
2011-12-02	RATCam	*r*	23:40	0.82–1.11	10.0	Good, ∼2
2011-12-25	X-shooter	–	00:58	0.85–2.25	606, 294, 100	Variable, ∼1
2012-01-08	RATCam	*i*	21:10	0.79–1.05	10.0	Good, ∼2
2012-01-14	RATCam	*i*	20:34	0.95–1.21	10.0	Good, ∼1.5
2012-01-18	ULTRACAM	*ugi*	19:43	0.29–1.47	4.0	Good, 1.5−3.0

(Bergeron & Leggett 2002). Recently, Kilic et al. (2012) used this approach to determine the cooling ages of the ultracool white dwarfs SDSS J1102+4113 and WD 0346+246, finding cooling ages of $10^{+0.4}_{-1.1}$ and $11.2^{+0.3}_{-1.6}$ Gyr, respectively. However, they still had to rely on the mass–radius relationship in order to determine all of their parameters. The majority of the ultracool white dwarfs have no parallaxes, and a canonical surface gravity of $\log g = 8$ was assumed for their analysis. However, altering this by a plausible ± 0.5 dex changes the resulting cooling age by several Gyr (Kilic et al. 2010b). Furthermore, the mass–radius relation for cool white dwarfs is all but untested observationally, further adding to the uncertainties. Hence, at present no ultracool white dwarf has a reliable mass determination, and their cooling ages are subject to large uncertainties.

One exception to this is the study of white dwarfs in star clusters. In the best cases the total age of the stars is well known as is the mass at the turnoff; hence, the mass at the tip of the white dwarf cooling sequence can be measured (Hansen et al. 2007). However, this picture is complicated by the presence of binaries (Bedin et al. 2008) and helium core white dwarfs (Kalirai et al. 2007), which add additional complexity to the white dwarf luminosity function. Furthermore, these white dwarfs cannot be used to constrain the age of the Galactic disc since they originated from a different population of stars.

Double-lined eclipsing binaries can be used to measure masses and radii with very few assumptions and to accuracies of better than 1 per cent (Andersen 1991; Southworth, Bruntt & Buzasi 2007), independent of model atmosphere calculations. This method has been applied to white dwarfs in eclipsing binaries and has resulted in the most precisely measured white dwarf masses and radii to date (Parsons et al. 2010, 2012a; Pyrzas et al. 2012). The subject of this paper, SDSS J013851.54−001621.6 (henceforth SDSS 0138−0016), was one of a number of candidate eclipsing white dwarf plus main-sequence binaries identified in the multi-epoch SDSS photometric survey, known as Stripe 82 (Becker et al. 2011).

Here we present high-precision photometry and spectroscopy of SDSS 0138−0016, confirming its binary and eclipsing nature, and use these data to directly measure the masses and radii of both stars in the binary. The same data also yield the temperature of the white dwarf and hence the age of the system.

2 OBSERVATIONS AND THEIR REDUCTION

2.1 William Herschel Telescope/ULTRACAM photometry

SDSS 0138−0016 was observed with ULTRACAM mounted as a visitor instrument on the 4.2 m William Herschel Telescope on 2011 November 1 and 2012 January 18. ULTRACAM is a high-speed, triple-beam CCD camera (Dhillon et al. 2007) which can acquire simultaneous images in three different bands; for our observations we used the SDSS *u*, *g* and either *r* or *i* filters. A complete log of these observations is given in Table 1. We windowed the CCD in order to achieve exposure times of ∼4 s which we varied to account for the conditions; the dead time between exposures was ∼25 ms. It is also possible to increase the exposure time of the *u*-band observations by co-adding the exposures on the CCD before readout. Since SDSS 0138−0016 is faint in this band ($u' = 20.55$), we used five co-adds for the *u*-band observations, resulting in exposure times of ∼20 s.

All of these data were reduced using the ULTRACAM pipeline software. Debiassing, flat-fielding and sky background subtraction were performed in the standard way. The source flux was determined with aperture photometry using a variable aperture, whereby the radius of the aperture is scaled according to the full width at half-maximum. Variations in observing conditions were accounted for by determining the flux relative to several comparison stars in the field of view. The data were flux calibrated by determining atmospheric extinction coefficients in each of the bands in which we observed and calculated the absolute flux of our target using observations of standard stars (Smith et al. 2002) taken in twilight. Using our extinction coefficients we extrapolated all fluxes to an airmass of 0. The systematic error introduced by our flux calibration is <0.1 mag in all bands.

2.2 Liverpool Telescope/RATCam photometry

Six primary eclipses of SDSS 0138−0016 were obtained in the *r* and *i* bands (three in each band) using RATCam, an optical CCD camera mounted on the robotic 2 m Liverpool Telescope (LT; Steele et al. 2004). Each eclipse observation was composed of 75 × 10 s exposures. We used 2 × 2 binning resulting in a readout time of ∼5 s between exposures. These observations are summarized in Table 1.

The raw data are automatically run through a pipeline that debiases, removes a scaled dark frame and flat-fields the data. The source flux was determined with aperture photometry using the ULTRACAM pipeline. The same nearby stars used to flux calibrate the ULTRACAM data were used to calibrate the RATCam data.

2.3 VLT/X-shooter spectroscopy

We obtained service mode observations of SDSS 0138−0016 with X-shooter (D'Odorico et al. 2006) mounted at the VLT-UT2 telescope. The observations were designed to cover an

entire orbit of the system. Details of these observations are listed in Table 1. X-shooter is a medium resolution spectrograph consisting of three independent arms that give simultaneous spectra longward of the atmospheric cutoff (0.3 μm) in the ultraviolet (the 'UVB' arm), optical (the 'VIS' arm) and up to 2.5 μm in the near-infrared (the 'NIR'arm). We used slit widths of 1.0, 0.9 and 0.9 arcsec in X-shooter's three arms binned by a factor of 2 in the dispersion direction in the UVB and VIS arms resulting in a spectral resolution of 2500–3500 across the entire spectral range.

The reduction of the raw frames was conducted using the standard pipeline release of the X-shooter Common Pipeline Library recipes (version 1.3.7) within ESOREX, the European Southern Observatory (ESO) Recipe Execution Tool, version 3.9.0. The standard recipes were used to optimally extract and wavelength calibrate each spectrum. The instrumental response was removed by observing the spectrophotometric standard star Feige 110 and dividing it by a flux table of the same star to produce the response function. The wavelength scale was also heliocentrically corrected.

3 RESULTS

3.1 Radial velocities

Fig. 1 shows the average spectrum for SDSS 0138−0016. The M star features dominate the spectrum, but there are also several emission lines that move in anti-phase to the absorption features of the M star. These emission lines originate from the white dwarf's chromosphere as a result of accretion of material from the wind of the M star. They have been seen in other close white dwarf plus main-sequence binaries and reliably track the motion of the white dwarf (Tappert et al. 2011a,b). A list of the unambiguously detected emission lines from the white dwarf is given in Table 2, though there are likely to be additional lines at longer wavelengths which are obscured by the dominant M star. A trailed spectrum of the Ca II 3934 Å line is shown in Fig. 2.

Each emission line was fitted with a combination of a first-order polynomial and a Gaussian component. For all the Balmer lines and the Ca II lines there is also an emission component from the M star due to activity, in all cases it is the emission component from the white dwarf that is stronger (see Fig. 2 for example). For these lines we fit both components simultaneously using a combination of a polynomial and two Gaussians. For the M star, we fit the K I 7700 Å absorption line. Although fits to other M star absorption features give consistent results, the K I 7700 Å line is the cleanest feature available. Fig. 3 shows sinusoidal fits to the measured radial velocities for both the white dwarf and the M star. Table 2 lists the fitted radial velocities for the white dwarf emission lines. We measure $K_1 = 86.5 \pm 1.0$ and $K_2 = 346.7 \pm 2.3\,\mathrm{km\,s^{-1}}$. The two radial velocity amplitudes give the mass ratio of the two stars $q = M_{\mathrm{sec}}/M_{\mathrm{WD}} = 0.249 \pm 0.003$.

Table 2. Identified white dwarf emission lines. γ_{WD} is the systemic velocity of the line and K_{WD} is the measured radial velocity of the line.

Line	Wavelength (Å)	γ_{WD} ($\mathrm{km\,s^{-1}}$)	K_{WD} ($\mathrm{km\,s^{-1}}$)
H 14	3721.948	108.5 ± 3.9	82.1 ± 4.2
H 13	3734.372	115.6 ± 7.3	74.6 ± 9.5
Fe I	3737.131	106.5 ± 3.3	87.0 ± 4.6
Fe I	3745.899	108.6 ± 2.8	85.3 ± 4.1
H 12	3750.152	109.1 ± 5.3	83.6 ± 7.7
H 11	3770.634	104.4 ± 3.8	84.4 ± 5.2
H 10	3797.910	105.7 ± 6.0	90.4 ± 8.8
H 9	3835.397	111.7 ± 7.6	78.8 ± 9.0
H 8	3889.055	100.4 ± 1.5	81.5 ± 2.5
Ca II	3933.663	105.0 ± 1.0	86.5 ± 1.0
Ca II	3968.469	106.6 ± 1.8	85.0 ± 2.8
Hϵ	3970.074	103.8 ± 1.1	87.0 ± 1.3
Hδ	4101.735	106.8 ± 1.1	87.5 ± 1.3
Ca I	4226.728	101.8 ± 8.3	80.4 ± 4.9
Hγ	4340.465	106.4 ± 1.0	87.3 ± 1.0
Fe I	4383.545	104.6 ± 1.8	84.0 ± 2.6
Hβ	4861.327	106.5 ± 0.5	87.0 ± 0.6
Mg I	5167.322	110.6 ± 6.6	88.8 ± 7.9
Mg I	5172.684	105.1 ± 1.7	87.1 ± 2.6
Mg I	5183.604	102.0 ± 1.2	85.9 ± 1.8
Hα	6562.760	104.5 ± 0.3	85.5 ± 0.4

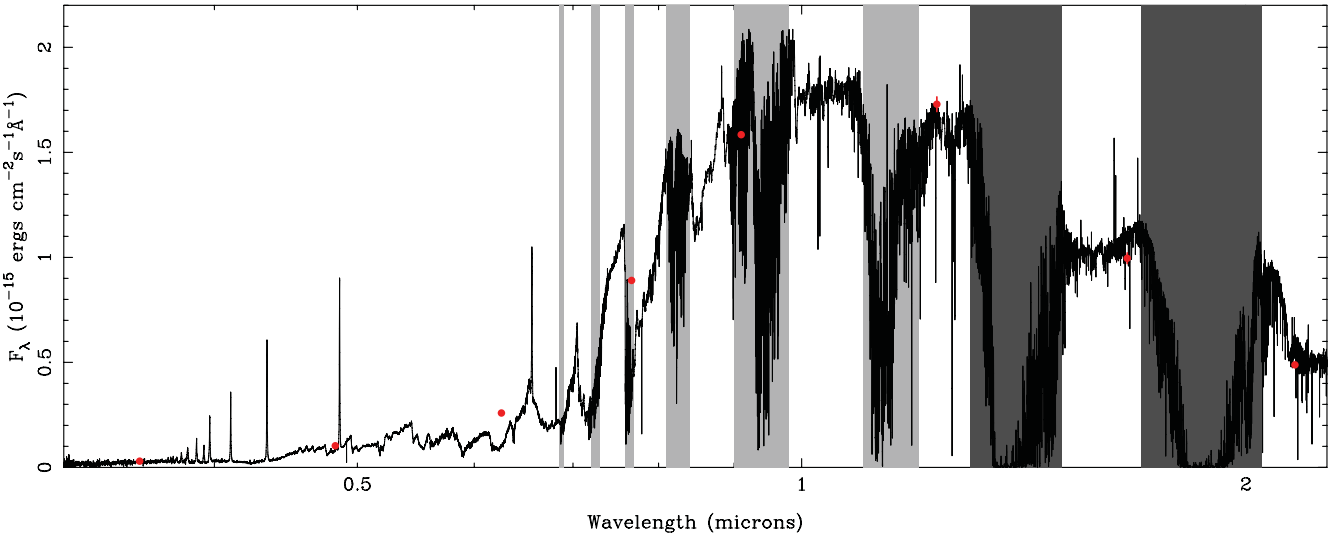

Figure 1. Averaged X-shooter spectrum of SDSS 0138−0016; no telluric correction has been applied. The grey regions cover areas of severe (light grey) or nearly complete (dark grey) telluric absorption. The red points are the SDSS *ugriz* and 2MASS *JHK* magnitudes.

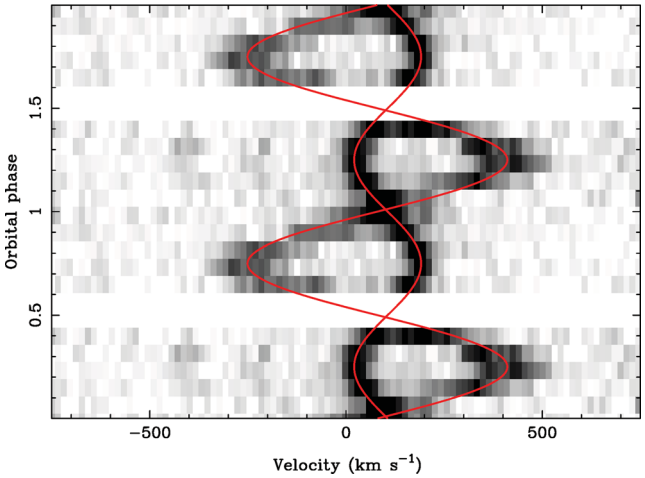

Figure 2. A trailed spectrum of the Ca II 3934 Å line. Emission can be seen from both components. The strongest component is from the white dwarf's chromosphere whilst the weaker (but larger amplitude) component originates from the main-sequence star. The red lines (online version only) track the motion of each component. Due to the short duration of the eclipse, the spectra taken at phase zero still cover the out-of-eclipse phase; hence, we are unable to say whether the white dwarf emission component is eclipsed. There was a 10 min gap in observations around phase 0.5, which was made for calibration reasons.

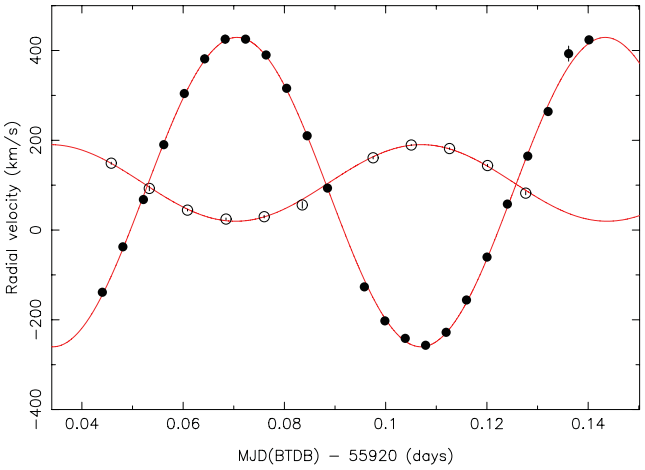

Figure 3. Radial velocity fits to the Ca II 3934 Å emission line from the white dwarf (open circles) and the K I 7700 Å absorption line from the M star (filled circles).

3.2 Light-curve model fitting

Fig. 4 shows our light curves of SDSS 0138−0016 around the expected time of the eclipse of the white dwarf by the M star. Our data confirm the eclipsing nature of the system. The reduced depth of the eclipse at longer wavelengths confirms that the bluer white dwarf is being eclipsed.

To measure the system parameters we fitted all the light curves using a code written for the general case of binaries containing white dwarfs (Copperwheat et al. 2010). It has been used in the study of other white dwarf main-sequence binaries (Parsons et al. 2010, 2012a; Pyrzas et al. 2012). The program subdivides each star into small elements with a geometry fixed by its radius as measured along the direction of centres towards the other star, Roche geometry distortion and beaming are also included. The code also calculates the white dwarf contribution to the overall flux.

The parameters needed to define the model were the mass ratio, $q = M_{\rm sec}/M_{\rm WD}$, the inclination, i, the stellar radii scaled by the orbital separation $R_{\rm sec}/a$ and $R_{\rm WD}/a$, quadratic limb darkening coefficients for both the stars, the time of mid-eclipse, T_0, the period, P and flux scaling factors for each star.

The primary eclipse shape does not contain enough information to determine the inclination and scaled radii of both stars simultaneously. However, the amplitude of the ellipsoidal modulation is related to the mass ratio and $R_{\rm sec}/a$. Therefore, since we knew the mass ratio from our spectroscopic observations we could use it as a prior constraint and hence we were able to measure these parameters simultaneously. Unfortunately, this approach did not work for the u-band data since the white dwarf dominates the overall flux in this band, suppressing the ellipsoidal modulation and making it much harder to fit. It is also of much lower signal-to-noise ratio and may be affected by activity from the M star. Since the RATCam light curves only covered the primary eclipse they could not be used to determine accurate parameters. However, we used them to measure the magnitudes of the two stars. We fitted all the RATCam light curves separately using the parameters found from the ULTRACAM light curves and allowed the flux scaling factors to vary.

For fitting the light curves, we phase folded the data and kept the period fixed as unity. The limb darkening of both stars was set using a four-coefficient formula:

$$I(\mu)/I(1) = 1 - \sum_{i=1}^{4} a_i(1 - \mu^{i/2}), \quad (1)$$

where μ is the cosine of the angle between the line of sight and the surface normal. For the secondary star, we use the coefficients for a $T_{\rm eff} = 2900$, $\log g = 5$ main-sequence star (Claret & Bloemen 2011). For the white dwarf we calculated the four coefficients from a white dwarf model atmosphere with $T_{\rm WD} = 3500$ and $\log g = 7.9$, folded through the appropriate filter profiles. We kept all limb darkening parameters fixed.

We used the Markov chain Monte Carlo (MCMC) method to determine the distributions of our model parameters (Press et al. 2007). The MCMC method involves making random jumps in the model parameters, with new models being accepted or rejected according to their probability computed as a Bayesian posterior probability. In this instance this probability is driven by a combination of χ^2 and the prior probability from our mass ratio constraint. Table 3 lists the best-fitting parameters and their statistical errors, along with the limb darkening coefficients used for both stars. All the fits to the g-, r- and i-band light curves give consistent results. Fig. 4 shows the fits to each band around the primary eclipse. We also show the best-fitting models but with the primary eclipse turned off, to illustrate the contribution of each star in the various bands.

The best-fitting model to the full light curve is shown in Fig. 5. We find an inclination of $77\overset{\circ}{.}19 \pm 0\overset{\circ}{.}02$ and a white dwarf mass and radius of $0.529 \pm 0.010\,{\rm M}_\odot$ and $0.0131 \pm 0.0003\,{\rm R}_\odot$, respectively. The surface gravity of the white dwarf is then $\log g = 7.926 \pm 0.022$.

4 WHITE DWARF TEMPERATURE AND AGE

Fig. 6 shows the SDSS spectrum of SDSS 0138−0016 in black and that of a second eclipsing white dwarf plus main-sequence binary SDSS 1210+3347 in grey (Pyrzas et al. 2012). These two systems

© 2012 The Authors, MNRAS **426,** 1950–1958
Monthly Notices of the Royal Astronomical Society © 2012 RAS

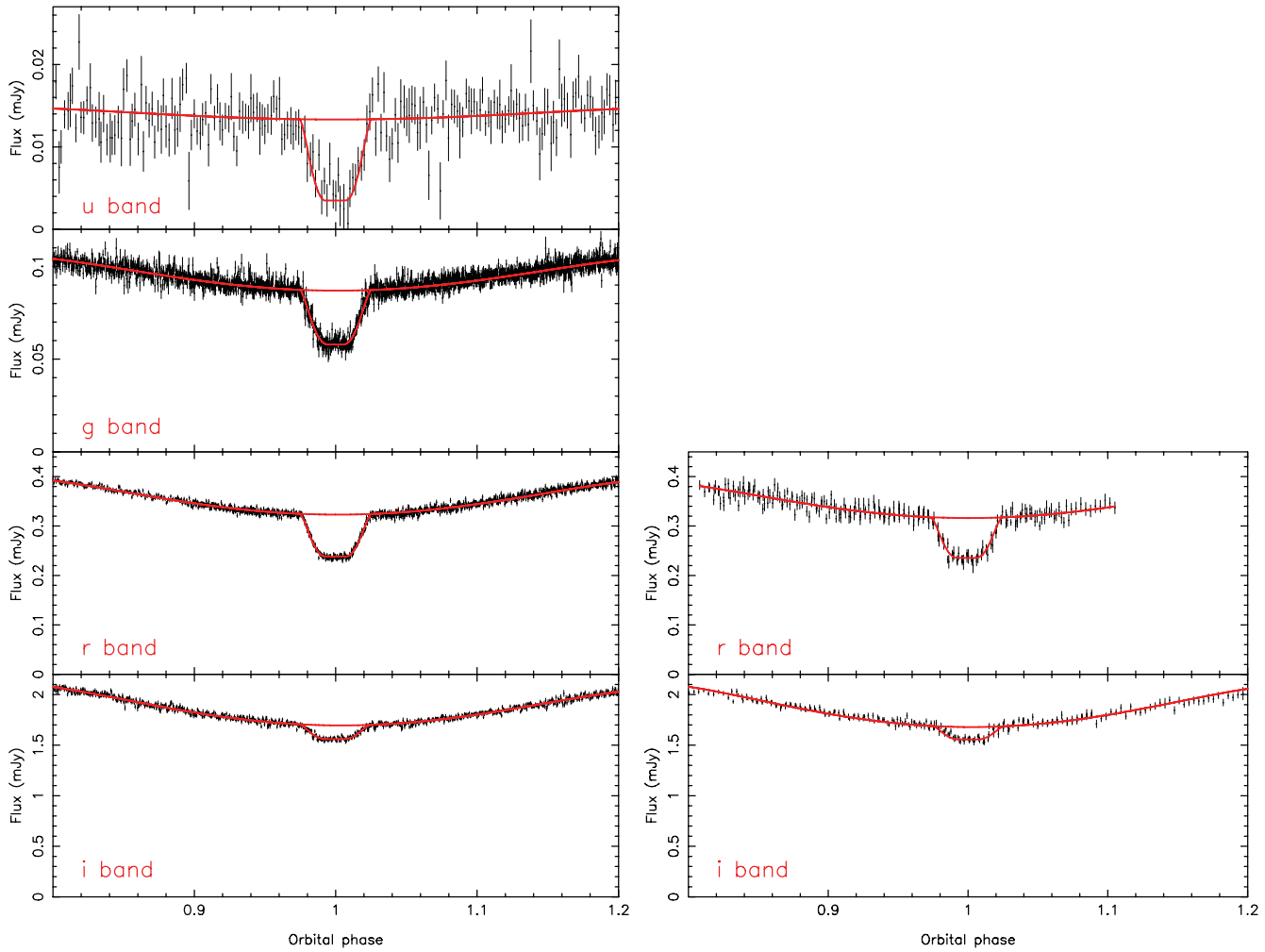

Figure 4. Primary eclipse light curves and fits. The data shown in the left-hand panels were obtained using ULTRACAM, whilst those in the right-hand panels are from RATCam. Two models are shown for each light curve, the best-fitting model and the same model but with no primary eclipse, demonstrating the relative contribution of each star in the different bands.

Table 3. Light-curve model parameters from MCMC minimization. The limb darkening coefficients (a_i) are also listed for each star.

Parameter	g	r	i
i	$77\overset{\circ}{.}14 \pm 0\overset{\circ}{.}04$	$77\overset{\circ}{.}19 \pm 0\overset{\circ}{.}02$	$77\overset{\circ}{.}25 \pm 0\overset{\circ}{.}07$
$r_{\rm WD}/a$	0.0200 ± 0.0007	0.0205 ± 0.0005	0.0212 ± 0.0018
$r_{\rm sec}/a$	0.333 ± 0.001	0.330 ± 0.001	0.328 ± 0.001
a_1 (WD)	-0.129	1.185	1.499
a_2 (WD)	2.710	-0.473	-0.402
a_3 (WD)	-3.079	-0.041	-0.457
a_4 (WD)	1.161	0.096	0.305
a_1 (sec)	0.2083	0.5288	0.6659
a_2 (sec)	1.1341	0.2451	0.5135
a_3 (sec)	-0.4029	0.4560	-0.2498
a_4 (sec)	0.0467	-0.2531	0.0307

are very similar since they contain M5 main-sequence stars and cool white dwarfs. Despite the low temperature of 6000 ± 200 K for the white dwarf in SDSS 1210+3347 a substantial blue excess is still produced (Pyrzas et al. 2012). No such excess is seen in the spectrum of SDSS 0138−0016 implying that the white dwarf is much cooler than the one in SDSS 1210+3347.

From our light-curve fits we measure white dwarf magnitudes of $g = 20.242 \pm 0.007$, $r = 19.079 \pm 0.006$ and $i = 18.773 \pm 0.020$. We also measure $u = 21.42 \pm 0.06$; however, the u-band magnitude is likely to be unreliable since we know that the M star is active and any activity on the M star will heavily affect the u band due to Balmer continuum emission. Therefore, we do not use the u-band magnitude to constrain the temperature of the white dwarf.

The colours of the white dwarf in SDSS 0138−0016 are shown in Fig. 7 along with those of other cool and ultracool white dwarfs (Harris et al. 1999, 2001; Hall et al. 2008; Kilic et al. 2010a,b; Leggett et al. 2011). We computed a set of model atmospheres spanning a wide range in effective temperatures and atmospheric He/H abundance ratios (Giammichele et al. 2012), we also include the opacity from the red wing of $L\alpha$. In all cases the mass was kept fixed as $0.529\,{\rm M}_{\odot}$. For low temperatures (<4000 K), the evolution of the cooling tracks in the $r - i$ colour depends almost exclusively on the temperature and in $g - r$ on the He/H abundance ratio. Ultracool white dwarfs become bluer in $r - i$ with decreasing temperature because of collisionally induced absorption and bluer in $g - r$ with increasing He/H ratio. The colours of the white dwarf in SDSS 0138−0016 therefore unambiguously constrain both its temperature, $T = 3570^{+110}_{-80}$ K, and its atmospheric composition, $\log({\rm He/H}) = 0.3$. The He abundance seems plausible, as we

© 2012 The Authors, MNRAS **426,** 1950–1958
Monthly Notices of the Royal Astronomical Society © 2012 RAS

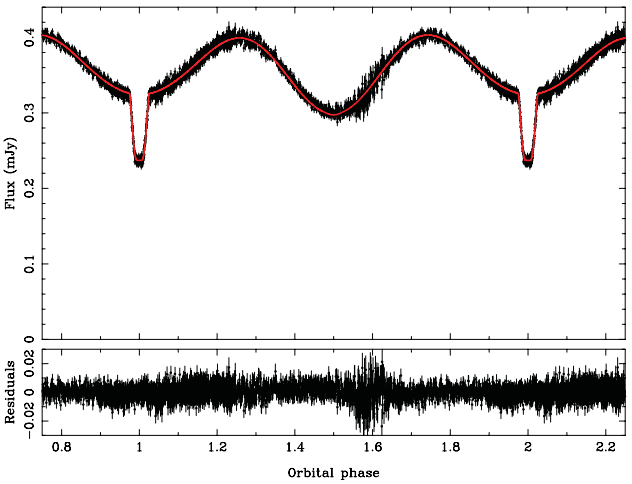

Figure 5. ULTRACAM *r*-band full orbit light curve of SDSS 0138−0016. The red line shows the best fit to the data. The out-of-eclipse variations are caused by the tidally distorted main-sequence star presenting a different surface area during the orbit. The amplitude of this modulation is related to the mass ratio ($q = M_{\rm sec}/M_{\rm WD}$) and the radius of the main-sequence star. Since we know the mass ratio from spectroscopy, the amplitude of the modulation, combined with the eclipse shape, allows us to measure the orbital inclination and radii of both stars. The lower panel shows the residuals to the fit; a small region of data was affected by clouds (around phase 1.6).

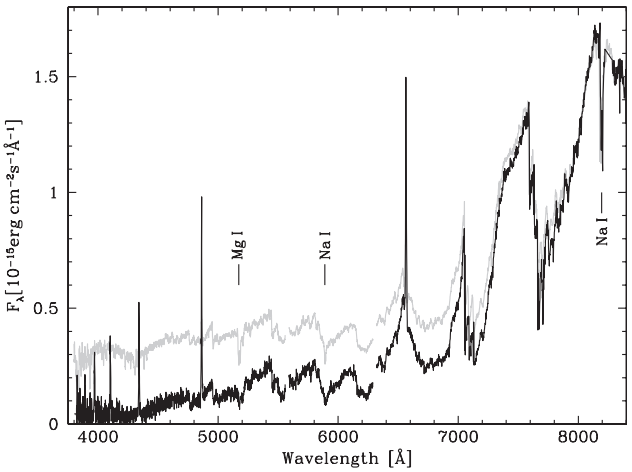

Figure 6. SDSS spectra of SDSS 0138−0016 (black line) and the similar eclipsing white dwarf plus main-sequence binary SDSS 1210+3347 (grey line) which contains a 6000 K white dwarf. Both of these systems contain an M5 main-sequence star and their spectra have been scaled to match in the *i* band. Therefore, any discrepancy at shorter wavelengths reflects differences in the white dwarf components.

know that the white dwarf is accreting from the wind of its H-rich companion, and that the accreted material will be mixed within the deep convection zone that is typical for very cool white dwarfs (Dufour et al. 2007). The model that best fits the measured colours of the white dwarf gives a surface gravity consistent with the value obtained from our light-curve fits. This internal consistency strongly supports the validity of our results and also independently confirms the accuracy of the mass–radius relationship of cool white dwarfs. Our final best-fitting model to the temperature and helium abundance implies a cooling age of $9.5^{+0.2}_{-0.3}$ Gyr for the white dwarf in SDSS 0138−0016, making it one of the oldest white dwarfs with an accurate cooling age.

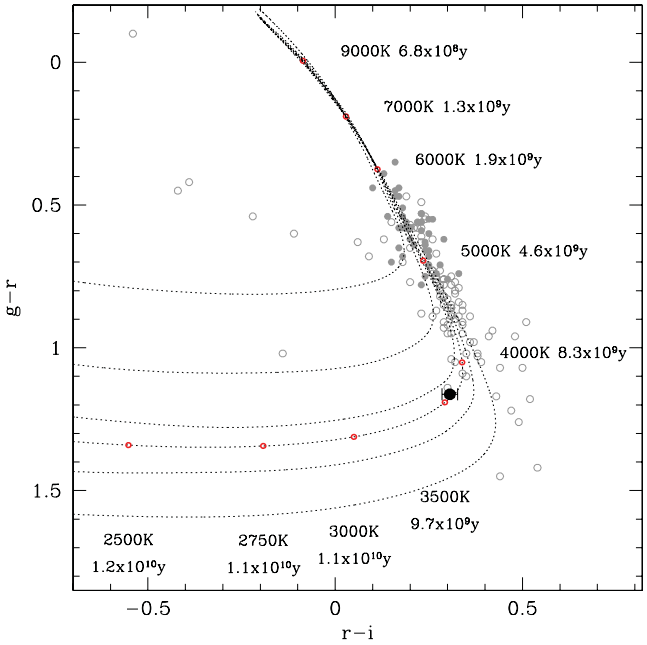

Figure 7. Colour–colour plot of cool white dwarfs. The dotted lines are cooling tracks for different atmospheric compositions, from top to bottom log(He/H) = 2.0, 1.0, 0.5, 0.3, 0.0 and − 1.0. In the calculation of these tracks, the mass of the white dwarf was fixed to 0.529 $M_\odot$, as determined from our spectroscopic and photometric fits. The best-model atmospheric fit is found for log (He/H) = 0.3 and $T = 3570^{+110}_{-80}$ K. Cooling ages and temperatures are given for the log (He/H) = 0.3, and we determine the age of the white dwarf in SDSS 0138−0016 to be $9.5^{+0.2}_{-0.3}$ Gyr. Furthermore, the surface gravity for this solution is in agreement with our measured value, meaning that the radius of the white dwarf in SDSS 0138−0016 is completely consistent with current mass–radius relationships.

5 DISTANCE AND KINEMATICS

We followed the prescription of Beuermann (2006) to estimate the distance of SDSS 0138−0016. For M dwarfs, the surface brightness near 7500 Å, and depth of the TiO band near 7165 Å are a strong function of the spectral type. Beuermann (2006) provides a calibration of the surface brightness $F_{\rm TiO}$ defined as the difference between the mean surface fluxes in the bands 7450–7550 and 7140–7190 Å. Measuring the observed flux $f_{\rm TiO}$ from the spectrum, the distance is then calculated as

$$d = \sqrt{R^2_{\rm sec}\frac{F_{\rm TiO}}{f_{\rm TiO}}}. \qquad (2)$$

Given the high accuracy of $R_{\rm sec}$ determined from the light-curve model, the main uncertainties in the distance estimate are the flux calibration of the spectroscopy and the spectral type of the companion. Adopting a conservative uncertainty in the spectral type of M5 ± 1.0, and using the SDSS and the VLT/X-shooter spectrum, we find a distance of 52^{+13}_{-10} pc, with the uncertainty in the spectral type dominating the error balance. Since the shape of the M dwarf in SDSS 0138−0016 is distorted by the white dwarf (see Section 6.1) we calculate the distance using the measured radius in several directions (and the spectra taken at the corresponding phase at which that radius is visible). We find that the oblateness of the M dwarf has a minor effect on the measured distance, much smaller than the uncertainty in the spectral type. The absolute magnitude of the white dwarf implied by this distance is $M_g = 16.66^{+0.46}_{-0.48}$, which is

© 2012 The Authors, MNRAS **426,** 1950–1958
Monthly Notices of the Royal Astronomical Society © 2012 RAS

in agreement with the best-fitting SED model, $M_g = 16.89$, further validating our results.

SDSS 0138−0016 has a relatively large proper motion ($\mu_\alpha = 336.2 \pm 3.8$, $\mu_\delta = 32.9 \pm 3.8$ mas yr^{-1}) and a systemic velocity, measured from the X-shooter spectra, of 84.5 ± 1.2 km s^{-1}. Using these values and the measured distance gives space velocities of $U = -99 \pm 9$, $V = +198 \pm 6$ and $W = -45 \pm 3$ km s^{-1}, which makes it likely that SDSS 0138−0016 is a member of the thick disc (Pauli et al. 2006).

6 DISCUSSION

6.1 System parameters

A full list of the physical parameters of SDSS 0138−0016 is given in Table 4. The secondary star's shape is highly distorted due to the presence of the nearby white dwarf. It fills 91 per cent of its Roche lobe (as measured towards the L1 point). Therefore, Table 4 lists the radius of the secondary star in various directions. For our final discussions we adopt the volume-averaged radii.

Fig. 8 shows the mass–radius plot for the white dwarf in SDSS 0138−0016. Also plotted are a number of theoretical mass–radius tracks from Benvenuto & Althaus (1999). Our measurements are in excellent agreement with the models, although not precise enough to distinguish between the different hydrogen layer masses. Nevertheless, this consistency reinforces our temperature and age measurement.

The mass–radius plot for low-mass stars is shown in Fig. 9. The measured mass and radius of the low-mass star in SDSS 0138−0016 are consistent with evolutionary models. Also shown are a number of other precise mass–radius measurements from low-mass stars that are in eclipsing binaries with white dwarfs. The precision of these measurements demonstrates the potential of these systems for testing low-mass stellar models. The number of these systems has increased rapidly in the last few years (Steinfadt, Bildsten & Howell 2008; Drake et al. 2009, 2010; Nebot Gómez-Morán et al. 2009; Pyrzas et al. 2009, 2012; Law et al. 2011) making them a valuable resource for testing the mass–radius relationship for low-mass stars.

As previously noted, the X-shooter spectra of SDSS 0138−0016 show emission components in the Balmer and Ca II lines originating from the M star due to activity (in addition to the components from the white dwarf). This indicates that the M star is still active, despite its age. The M5 star has an age of at least 9.5 Gyr, likely more than 10 Gyr when the main-sequence lifetime of the white dwarf progenitor is taken into account. West et al. (2008) list the activity lifetime of an M5 star as 7.0 ± 0.5 Gyr, substantially shorter than the age of the M star in SDSS 0138−0016. Therefore, it is likely that the tidally induced rapid rotation of the M star keeps it active and makes it appear younger.

Table 4. System parameter of SDSS 0138−0016.

Parameter	Value
Orbital period	0.072 76491(2) d
T_0 [MJD(BTDB)]	558 67.007 405(6)
Orbital separation	0.639 ± 0.004 R$_\odot$
Orbital inclination	$77.19^\circ \pm 0.02^\circ$
White dwarf mass	0.529 ± 0.010 M$_\odot$
White dwarf radius	0.0131 ± 0.0003 R$_\odot$
White dwarf log g	7.926 ± 0.022
White dwarf effective temperature	3570^{+110}_{-80} K
White dwarf cooling age	$9.5^{+0.2}_{-0.3}$ Gyr
Secondary star mass	0.132 ± 0.003 M$_\odot$
Secondary star radius substellar	0.211 ± 0.001 R$_\odot$
Secondary star radius polar	0.157 ± 0.001 R$_\odot$
Secondary star radius backside	0.183 ± 0.001 R$_\odot$
Secondary star radius side	0.163 ± 0.001 R$_\odot$
Secondary star radius volume averaged	0.165 ± 0.001 R$_\odot$
Distance	52^{+13}_{-10} pc

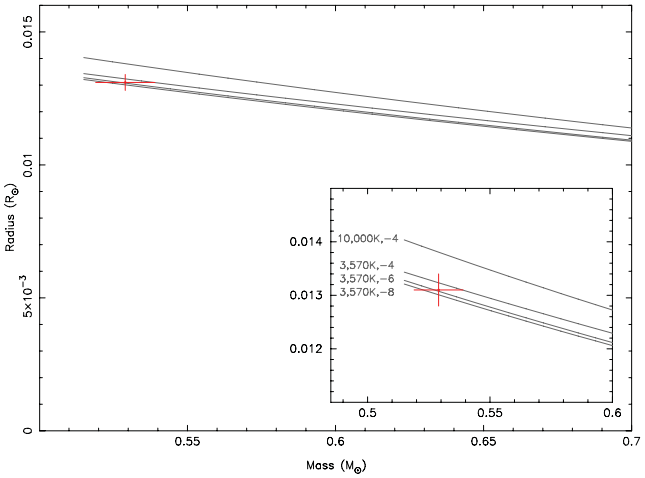

Figure 8. Mass–radius plot for the white dwarf in SDSS 0138−0016. The grey lines are theoretical mass–radius tracks from Benvenuto & Althaus (1999) where the first number is the temperature of the white dwarf and the second number is the exponent of the hydrogen layer fraction.

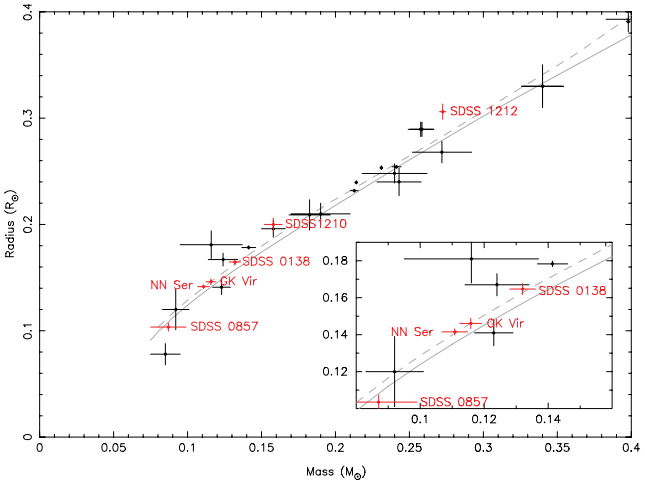

Figure 9. Mass–radius plot for low-mass stars. The mass and radius values for the M star in SDSS 0138−0016 are shown as well as others from eclipsing white dwarf binaries in red (Parsons et al. 2010, 2012a,b; Pyrzas et al. 2012). Other measurements are from Knigge, Baraffe & Patterson (2011), Carter et al. (2011) and Ofir et al. (2012). The solid line is the 8 Gyr isochrone from Baraffe et al. (1998) whilst the dashed line is a 5 Gyr model from Morales et al. (2010) which includes the effects of magnetic activity. Also shown is a zoom in on the region around SDSS 0138−0016.

6.2 Evolution of the system

We reconstruct the past and future evolution of SDSS 0138−0016 using the tools described in Schreiber & Gänsicke (2003), Zorotovic et al. (2010) and Zorotovic, Schreiber & Gänsicke (2011).

Assuming that the only mechanism of angular momentum loss from the system is via gravitational radiation then

SDSS 0138−0016 emerged from the common envelope 9.5 Gyr ago with an orbital period of 5.28 h.

Fixing the common envelope efficiency to $\alpha = 0.25$ results in a mass of the white dwarf progenitor of 1.83 $M_\odot$. The evolutionary time-scale of the white dwarf progenitor in this case would have been 1.63 Gyr, giving a total age of the system of 11.13 Gyr. Allowing for values of α between 0 and 1 but insisting that the evolutionary time-scale of the progenitor is less than 4 Gyr (i.e. the system must be younger than 13.5 Gyr), leads to a range of progenitor masses between 1.39 and 2.00 $M_\odot$.

A total age of ∼11 Gyr makes it more likely that SDSS 0138−0016 is a member of the thick disc (as the space motion implies). This makes it a fairly old member of this population but consistent with previous kinematic studies that found that thick disc stars have a mean age of 10 ± 2 Gyr (Feltzing & Bensby 2009). However, there is still some uncertainty as to whether the Galaxy has a thick–thin disc bimodality (Bovy, Rix & Hogg 2012).

The continuing loss of orbital angular momentum will lead SDSS 0138−0016 to become a cataclysmic variable in 70 Myr at which point it will have an orbital period of 1.66 h. Due to the long angular momentum loss time-scale, systems of this type, so close to mass transfer, are likely to be rare.

7 CONCLUSIONS

Using high-precision photometric and spectroscopic data we measure the mass and radius of the ultracool white dwarf and low-mass star in the eclipsing binary SDSS 0138−0016. We use this information and the colour of the white dwarf to determine its atmospheric composition, temperature and age. We find that the white dwarf has a temperature of 3570^{+110}_{-80} K and has been cooling for $9.5^{+0.2}_{-0.3}$ Gyr. We also find that the mass and radius measurements for both the ultracool white dwarf and the low-mass star are consistent with evolutionary models. This supports the use of theoretical white dwarf mass–radius relationships when attempting to determine the temperature of ultracool white dwarfs using SED fitting and parallax measurements.

We find that the activity lifetime of the main-sequence star has been greatly extended due to being forced to rapidly rotate. The system is very close to Roche lobe overflow and will become a cataclysmic variable in only 70 Myr.

The opacity from collisionally induced absorption from hydrogen in the ultracool white dwarf atmosphere is strongest in the near-infrared, making this wavelength range particularly sensitive to the temperature and atmospheric composition. Therefore, future measurements of the near-infrared magnitudes for the white dwarf will improve the precision and accuracy of the temperature and composition of the white dwarf.

ACKNOWLEDGMENTS

We thank the referee, David Pinfield, for his useful comments and suggestions. SGP acknowledges support from the Joint Committee ESO-Government of Chile. ULTRACAM, BTG, TRM, CMC, VSD and SPL are supported by the Science and Technology Facilities Council (STFC). MRS acknowledges support from FONDECYT (1100782) and Millennium Science Initiative, Chilean Ministry of Economy: Nucleus P10-022-F. The results presented in this paper are based on observations collected at the European Southern Observatory under programme ID 288.D-5015. The LT is operated on the island of La Palma by Liverpool John Moores University in the Spanish Observatorio del Roque de los Muchachos of the Instituto de Astrofisica de Canarias with financial support from the UK Science and Technology Facilities Council.

REFERENCES

Andersen J., 1991, A&AR, 3, 91
Baraffe I., Chabrier G., Allard F., Hauschildt P. H., 1998, A&A, 337, 403
Becker A. C., Bochanski J. J., Hawley S. L., Ivezić Ž., Kowalski A. F., Sesar B., West A. A., 2011, ApJ, 731, 17
Bedin L. R., Salaris M., Piotto G., Cassisi S., Milone A. P., Anderson J., King I. R., 2008, ApJ, 679, L29
Benvenuto O. G., Althaus L. G., 1999, MNRAS, 303, 30
Bergeron P., Leggett S. K., 2002, ApJ, 580, 1070
Bergeron P., Ruiz M.-T., Leggett S. K., Saumon D., Wesemael F., 1994, ApJ, 423, 456
Bergeron P., Saumon D., Wesemael F., 1995, ApJ, 443, 764
Beuermann K., 2006, A&A, 460, 783
Bovy J., Rix H.-W., Hogg D. W., 2012, ApJ, 751, 131
Carter J. A. et al., 2011, Sci, 331, 562
Claret A., Bloemen S., 2011, A&A, 529, A75
Copperwheat C. M., Marsh T. R., Dhillon V. S., Littlefair S. P., Hickman R., Gänsicke B. T., Southworth J., 2010, MNRAS, 402, 1824
D'Odorico S. et al., 2006, Proc. SPIE, 6269, 98
Day-Jones A. C. et al., 2008, MNRAS, 388, 838
Dhillon V. S. et al., 2007, MNRAS, 378, 825
Drake A. J. et al., 2009, ApJ, 696, 870
Drake A. J. et al., 2010, preprint (arXiv:e-prints)
Dufour P. et al., 2007, ApJ, 663, 1291
Feltzing S., Bensby T., 2009, in Mamajek E. E., Soderblom D. R., Wyse R. F. G., eds, Proc. IAU Symp. 258, The age of stars. Cambridge Univ. Press, Cambridge, p. 23
Fontaine G., Brassard P., Bergeron P., 2001, PASP, 113, 409
Giammichele N., Bergeron P., Dufour P., 2012, ApJS, 199, 29
Girven J., Gänsicke B. T., Steeghs D., Koester D., 2011, MNRAS, 417, 1210
Hall P. B., Kowalski P. M., Harris H. C., Awal A., Leggett S. K., Kilic M., Anderson S. F., Gates E., 2008, AJ, 136, 76
Hansen B. M. S. et al., 2007, ApJ, 671, 380
Harris H. C., Dahn C. C., Vrba F. J., Henden A. A., Liebert J., Schmidt G. D., Reid I. N., 1999, ApJ, 524, 1000
Harris H. C. et al., 2001, ApJ, 549, L109
Kalirai J. S., Bergeron P., Hansen B. M. S., Kelson D. D., Reitzel D. B., Rich R. M., Richer H. B., 2007, ApJ, 671, 748
Kilic M. et al., 2010a, ApJS, 190, 77
Kilic M. et al., 2010b, ApJ, 715, L21
Kilic M., Thorstensen J. R., Kowalski P. M., Andrews J., 2012, MNRAS, 423, L132
Knigge C., Baraffe I., Patterson J., 2011, ApJS, 194, 28
Law N. M. et al., 2011, preprint (arXiv:e-print)
Leggett S. K., Lodieu N., Tremblay P.-E., Bergeron P., Nitta A., 2011, ApJ, 735, 62
Morales J. C., Gallardo J., Ribas I., Jordi C., Baraffe I., Chabrier G., 2010, ApJ, 718, 502
Nebot Gómez-Morán A. et al., 2009, A&A, 495, 561
Ofir A., Gandolfi D., Buchhave L., Lacy C. H. S., Hatzes A. P., Fridlund M., 2012, MNRAS, 423, L1
Parsons S. G., Marsh T. R., Copperwheat C. M., Dhillon V. S., Littlefair S. P., Gänsicke B. T., Hickman R., 2010, MNRAS, 402, 2591
Parsons S. G. et al., 2012a, MNRAS, 420, 3281
Parsons S. G. et al., 2012b, MNRAS, 419, 304
Pauli E.-M., Napiwotzki R., Heber U., Altmann M., Odenkirchen M., 2006, A&A, 447, 173
Pinfield D. J., Jones H. R. A., Lucas P. W., Kendall T. R., Folkes S. L., Day-Jones A. C., Chappelle R. J., Steele I. A., 2006, MNRAS, 368, 1281
Press W. H., Teukolsky A. A., Vetterling W. T., Flannery B. P., 2007, Numerical Recipes: The Art of Scientific Computing, 3rd edn. Cambridge Univ. Press, Cambridge

Pyrzas S. et al., 2009, MNRAS, 394, 978
Pyrzas S. et al., 2012, MNRAS, 419, 817
Schreiber M. R., Gänsicke B. T., 2003, A&A, 406, 305
Smith J. A. et al., 2002, AJ, 123, 2121
Southworth J., Bruntt H., Buzasi D. L., 2007, A&A, 467, 1215
Steele I. A. et al., 2004, Proc. SPIE, 5489, 679
Steele P. R., Burleigh M. R., Dobbie P. D., Jameson R. F., Barstow M. A., Satterthwaite R. P., 2011, MNRAS, 416, 2768
Steinfadt J. D. R., Bildsten L., Howell S. B., 2008, ApJ, 677, L113
Tappert C., Gänsicke B. T., Rebassa-Mansergas A., Schmidtobreick L., Schreiber M. R., 2011a, A&A, 531, A113
Tappert C., Gänsicke B. T., Schmidtobreick L., Ribeiro T., 2011b, A&A, 532, A129
West A. A., Hawley S. L., Bochanski J. J., Covey K. R., Reid I. N., Dhital S., Hilton E. J., Masuda M., 2008, AJ, 135, 785
Zorotovic M., Schreiber M. R., Gänsicke B. T., Nebot Gómez-Morán A., 2010, A&A, 520, A86
Zorotovic M., Schreiber M. R., Gänsicke B. T., 2011, A&A, 536, A42

This paper has been typeset from a TEX/LATEX file prepared by the author.